PERGAMON

International Journal of Solids and Structures 38 (2001) 6405–6426

INTERNATIONAL JOURNAL OF SOLIDS and STRUCTURES

www.elsevier.com/locate/ijsolstr

Mode decomposition of three-dimensional mixed-mode cracks via two-state integrals

Young Jong Kim, Hyun-Gyu Kim, Seyoung Im *

Department of Mechanical Engineering, Korea Advanced Institute of Science and Technology (KAIST), Science Town, Taejon 305-701, South Korea

Received 6 July 2000

Abstract

A numerical scheme is proposed to obtain the individual stress intensity factors in an axisymmetric crack and in a three-dimensional mixed-mode crack. The procedures presented here are based on the path independence of J and M integrals and mutual or two-state conservation integrals, which involve two elastic fields. A useful method to decompose the stress intensity factors along curved three-dimensional cracks under mixed mode is derived by using appropriate auxiliary fields for the plane problems. The choice of the auxiliary fields available is critical to success of the present scheme, and in this study it is made of not only the asymptotic plane-strain solution, which requires some remedy in application of the two-state integral due to the lack of equilibrium and compatibility, but a numerical solution with a given stress intensity as well. Some numerical examples of penny-shaped cracks are presented to investigate the applicability and effectiveness of the method for problems of axisymmetric and three-dimensional cracks.

Keywords: Mode decomposition; Stress intensity factors; J integral; Mutual integral; Auxiliary field; Three-dimensional crack; Penny-shaped crack

1. Introduction

Conservation integrals in elasticity have been widely applied to the fracture mechanics, among which the J integral is the most popular one. The J integral is path independent and has been shown to be identical to Irwin's energy release rate associated with the collinear extension of a crack in an elastic solid (Rice, 1968). It has been related to the crack tip stress intensity factors in both linear and nonlinear elastic solids subjected to infinitesimal deformations (Hutchinson, 1968). It is necessary to evaluate the individual stress intensity factors separately for mixed-mode crack problems in order to investigate the crack growth and the crack propagation. However, the evaluation of the J integral alone does not determine the individual stress intensity factors, K_{I}, K_{II} and K_{III} separately.

* Corresponding author. Tel.: +82-42-869-3028; fax: +82-42-861-0919.
E-mail addresses: yjkim@imhp.kaist.ac.kr (Y.J. Kim), khg@imhp.kaist.ac.kr (H.-G. Kim), sim@mail.kaist.ac.kr (S. Im).

0020-7683/01/$ - see front matter
PII: S0020-7683(00)00408-X

Many works on mixed-mode crack problems using the path-independent integrals have been reported. Bui (1983) developed a technique using the J integral associated with Mode I and Mode II, in which the symmetric and antisymmetric parts of the planar displacement, strain and stress fields about the crack plane are separated. Stern et al. (1976) employed another conservation integral based on Betti's reciprocal work theorem with known auxiliary fields. Later the method was extended for the straight interfacial cracks by Hong and Stern (1978). For planar cracks, Yau et al. (1980), Wang and Yau (1981) and Shih and Asaro (1988) utilized a new class of conservation integral known as mutual integral or two-state conservation integral, proposed by Eshelby (1956) and later by Chen and Shield (1977): Nakamura and Parks (1989) and Nakamura (1991) employed the same approach to determine the mixed-mode stress intensity factors for three-dimensional interface crack problems. Nikishkov and Atluri (1987a) developed a domain integral approach to calculate mixed-mode stress intensity factors for planar three-dimensional cracks. Nahta and Moran (1993) and Gosz et al. (1998) used asymptotic auxiliary fields for the plane problems to decompose the stress intensity factors in mixed-mode cracks, and proposed a method to evaluate the divergence term in the two-state integral. Choi and Earmme (1992) employed the two-state L integral to evaluate the stress intensity factors in circular arc-shaped interfacial crack. Recently Im and Kim (2000) showed that the two-state M integral is applicable for computing the intensity of the singular near-tip field for a generic isotropic composite wedge including planar cracks. The main interest of fracture mechanics is shifting from two- to three-dimensional crack problems and particularly it becomes increasingly important to study three-dimensional mixed-mode crack problems for the crack growth and propagation prediction.

This study presents a method to obtain the individual stress intensity factors for axisymmetric and three-dimensional cracks in mixed mode. The method is based on the path independence of J and M and two-state J integral, which involves two independent elastic fields. The path independence of these conservation integrals enables one to obtain each stress intensity factor from the displacements and stresses remote from the crack tip. In this paper, we present a simple method to evaluate the two-state integral with asymptotic auxiliary fields for the plane problems. In particular, the divergence term in the two-state integral, which arises due to the lack of equilibrium and compatibility of asymptotic auxiliary fields, is reduced to a simple form, with the aid of the equilibrium equation for the plane problems, by imposing displacements of asymptotic solutions on the nodes of finite elements. Numerical auxiliary fields, finite element solutions for penny-shaped crack problems under pure Mode I and Mode III, are used to obtain reference stress intensity factors in three-dimensional mixed-mode cracks. The purpose of this study is to show the validity of the numerical auxiliary fields and the effectiveness of the present method to calculate the divergence term in the two-state integral for mode decomposition utilizing the auxiliary field of the plane-strain asymptotic solution. In Section 2 the basic formulation for the method is described and the solution procedure is established. The implementation of the scheme is explained in Section 3, and numerical examples are carried out in Section 4.

2. Formulation of the problems

2.1. Axisymmetric formulation

In three-dimensional infinitesimal deformations of homogeneous isotropic bodies, M integral is defined as (Knowles and Sternberg, 1972)

$$M = \int_A \left(W x_i n_i - T_i u_{i,j} x_j - \frac{1}{2} T_i u_i \right) \mathrm{d}A \quad (i = 1, 2, 3), \tag{1}$$

where W is the strain energy density, u_i is the displacement, n_i is the unit outward normal vector, T_i is the traction vector, and A indicates a surface.

Consider crack problems in an elastic, homogeneous, isotropic axisymmetric solid under axisymmetric loading conditions. As a result of its axisymmetry, Eq. (1) can then be rewritten as (Kuo, 1987)

$$M = 2\pi \int_C \left(W x_\alpha n_\alpha - T_\alpha u_{\alpha,\beta} x_\beta - \frac{1}{2} T_\alpha u_\alpha \right) x_1 \, \mathrm{d}s, \tag{2}$$

where the subscripts α and β indicate the components in the r–z or the x_1–x_2 plane (see Fig. 1), and C encloses the crack tip (it may be taken to be C_1 or C_2 in Fig. 1). Note that x_1 and x_2 are used for r and z whenever it is convenient to do so. Physically, Eq. (2) implies that M integral is a driving force for a crack to expand uniformly (Budiansky and Rice, 1973).

Straightforward argument reveals that the M integral has the following relationships for the axisymmetric cracks (Kuo, 1987) in the absence of Mode III or torsion.

$$J = J_{\mathrm{I}} + J_{\mathrm{II}} \tag{3}$$

with

$$J_{\mathrm{I}} = \frac{M_{\mathrm{I}}}{2\pi r_{\mathrm{c}}^2} = \alpha K_{\mathrm{I}}^2 \quad \text{and} \quad J_{\mathrm{II}} = \frac{M_{\mathrm{II}}}{2\pi r_{\mathrm{c}}^2} = \alpha K_{\mathrm{II}}^2,$$

where $\alpha = (1 - \nu^2)/E$ (E: Young's modulus; ν: Poisson's ratio), and r_{c} is the r or the x_1 coordinate of the crack tip, that is, the shortest distance from the z axis to the crack tip.

It should be noted here that the J integral in Eq. (3) alone does not provide adequate information for determining the individual stress intensity factors K_{I} and K_{II} in a mixed-mode crack problem. Following Chen and Shield (1977), we consider two independent elastic states of a penny-shaped crack: the field of the target problem denoted by superscript "(1)" and an auxiliary field denoted by "(2)". Let the elastic state from the superposition of the two elastic fields be denoted by superscript "(0)". Then the J integral for the resulting state has the following form:

$$J^{(0)} = J^{(1)} + J^{(2)} + J^{(1,2)} \tag{4}$$

in which $J^{(1)}$, $J^{(2)}$ and $J^{(1,2)}$ are given as

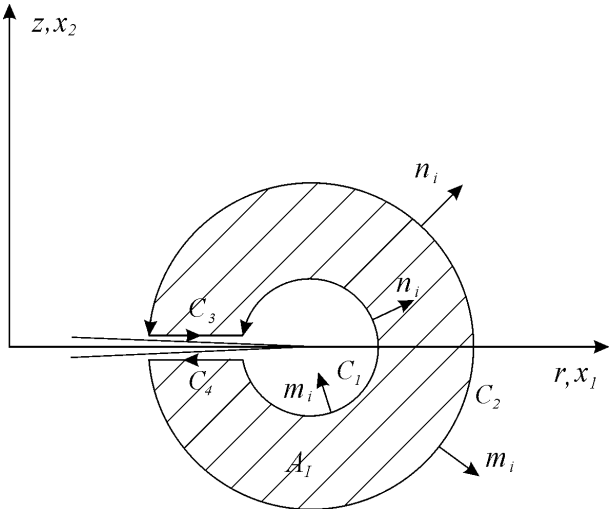

Fig. 1. Simply connected region A_{I} enclosed by the contour C on the cross-section of an axisymmetric crack.

$$J^{(a)} = \frac{1}{r_c^2}\int_C F_m^{(a)} n_m x_1 \,\mathrm{d}s \quad (a = 1, 2), \tag{5a}$$

$$J^{(1,2)} = \frac{1}{r_c^2}\int_C F_m^{(1,2)} n_m x_1 \,\mathrm{d}s \tag{5b}$$

with

$$F_m^{(a)} = W^{(a)} x_i \delta_{im} - \sigma_{ik}^{(a)} u_{i,j}^{(a)} x_j \delta_{km} - \tfrac{1}{2}\sigma_{kn}^{(a)} u_k^{(a)} \delta_{nm},$$

$$F_m^{(1,2)} = W^{(1,2)} x_i \delta_{im} - \left(\sigma_{ik}^{(1)} u_{i,j}^{(2)} + \sigma_{ik}^{(2)} u_{i,j}^{(1)}\right) x_j \delta_{km} - \tfrac{1}{2}\left(\sigma_{kn}^{(1)} u_k^{(2)} + \sigma_{kn}^{(2)} u_k^{(1)}\right) \delta_{nm},$$

where δ_{ij} is the Kronecker delta and $W^{(1,2)}$ is the two-state strain energy density of the elastic body, defined by

$$W^{(1,2)} = C_{ijkl} u_{i,j}^{(1)} u_{k,l}^{(2)} = C_{ijkl} u_{i,j}^{(2)} u_{k,l}^{(1)}. \tag{6}$$

In Eqs. (5a) and (5b), $\sigma_{ij}^{(1)}$ and $u_i^{(1)}$ can be obtained from analytic or numerical solution to the target problem along a properly selected integration path C, while $\sigma_{ij}^{(2)}$ and $u_i^{(2)}$ are given from the auxiliary field, which is chosen in a convenient manner.

Recalling the relationships of Eq. (3), one finds that the J integral for the state "(0)" is expressed as

$$J^{(0)} = \alpha\left\{\left[K_{\mathrm{I}}^{(1)} + K_{\mathrm{I}}^{(2)}\right]^2 + \left[K_{\mathrm{II}}^{(1)} + K_{\mathrm{II}}^{(2)}\right]^2\right\}, \tag{7}$$

which leads to

$$J^{(0)} = J^{(1)} + J^{(2)} + 2\alpha\left(K_{\mathrm{I}}^{(1)} K_{\mathrm{I}}^{(2)} + K_{\mathrm{II}}^{(1)} K_{\mathrm{II}}^{(2)}\right). \tag{8}$$

Comparison between Eqs. (4) and (8) reveals that

$$J^{(1,2)} = 2\alpha\left(K_{\mathrm{I}}^{(1)} K_{\mathrm{I}}^{(2)} + K_{\mathrm{II}}^{(1)} K_{\mathrm{II}}^{(2)}\right). \tag{9}$$

The J integral shown in Eqs. (5b) and (9) deals with the interaction term only and is to be used for solving mixed-mode penny-shaped crack problems in a linear elastic solid. It should be noted here that the $J^{(1,2)}$ integral is related to the details of the stresses and deformation at the crack tip (i.e., K_{I} and K_{II} in Eq. (9)). Due to the path independence of this integral, however, it may be evaluated in the region away from the crack tip (i.e., the integral in Eq. (5b)), where such a calculation can be carried out with greater accuracy and convenience than near the crack tip.

Eq. (5b) together with Eq. (9) provides, in fact, sufficient information for determining the stress intensity factors for a mixed-mode fracture problem of a penny-shaped crack, when a proper known auxiliary field is introduced. Let the superscript "(2a)" indicate the solution for an auxiliary elastic field, wherein the body under consideration is in the state of Mode I deformation only, i.e.,

$$K_{\mathrm{I}}^{(2a)} \neq 0 \quad \text{and} \quad K_{\mathrm{II}}^{(2a)} = 0. \tag{10}$$

Eq. (9) can be simplified as

$$J^{(1,2a)} = 2\alpha K_{\mathrm{I}}^{(1)} K_{\mathrm{I}}^{(2a)}. \tag{11}$$

For the target problem field and for the auxiliary field of Mode I, we have, respectively:

$$J^{(1)} = \alpha\left\{\left[K_{\mathrm{I}}^{(1)}\right]^2 + \left[K_{\mathrm{II}}^{(1)}\right]^2\right\}, \qquad J^{(2a)} = \alpha\left[K_{\mathrm{I}}^{(2a)}\right]^2. \tag{12}$$

Eqs. (11) and (12) leads to the expressions of the individual stress intensity factors for the target field in terms of the conservation integrals, $J^{(1)}$, $J^{(2a)}$ and $J^{(1,2a)}$:

$$K_{\mathrm{I}}^{(1)} = \frac{J^{(1,2a)}}{2\sqrt{\alpha J^{(2a)}}} \quad \text{and} \quad K_{\mathrm{II}}^{(1)} = \pm\sqrt{\frac{1}{\alpha}}\sqrt{J^{(1)} - \frac{\left[J^{(1,2a)}\right]^2}{4J^{(2a)}}}. \tag{13}$$

It should be noted that the integrals $J^{(1)}$, $J^{(2a)}$ and $J^{(1,2a)}$ have to be calculated accurately for proper evaluation of $K_{\mathrm{I}}^{(1)}$ and $K_{\mathrm{II}}^{(1)}$. For a given crack geometry and loading condition, this can be achieved by integrating Eqs. (5a) and (5b) along a properly selected band in the far field utilizing the domain integral expression (Li et al., 1985; Nikishkov and Atluri, 1987b).

2.2. Three-dimensional formulation

In three-dimensional infinitesimal deformation of homogeneous isotropic elastic bodies the energetic force J_k integral is given as (Eshelby, 1956; Knowles and Sternberg, 1972)

$$J_k = \int_A (Wn_k - T_i u_{i,k})\,\mathrm{d}A = \int_A H_{kj} n_j\,\mathrm{d}A, \tag{14}$$

where A indicates a surface surrounding the crack front as in Fig. 2, and it includes the crack surfaces as well as the remaining boundary so that $A = S_{\mathrm{o}}$; the integrand H_{kj} is the energy momentum tensor, given as $W\delta_{kj} - \sigma_{ij}u_{i,k}$. Note that the pointwise value of J along the crack front is required for mode decomposition. Let $J(s)$ indicate the energy release rate associated with the self-similar crack growth on the crack front. As the cylindrical surface A shrinks to the crack front line (Moran and Shih, 1987), $J(s)$ is given as

$$J(s) = \frac{-\lim_{\Gamma\to 0}\int_{S_{\mathrm{t}}} l_k H_{kj} m_j\,\mathrm{d}A}{\int_{L_{\mathrm{c}}} l_k v_k\,\mathrm{d}s}, \tag{15}$$

where "Γ" is the circular contour on the r–z plane that represents the cross-section of the shrinking surface S_{t} (see Fig. 2c); "s" denotes the coordinate along the crack front of a three-dimensional crack; l_k, which is short for $l_k(s)$, indicates the component of crack advance vector (see Fig. 2b); v_k, which is short for $v_k(s)$, represents an outward unit vector normal to crack front on the crack plane and m_j is the normal to Γ pointing towards the crack front; i.e., $m_j = -n_j$ on Γ as shown in Fig. 2a. Furthermore, L_{c} is a small interval on the line of the crack front for virtual crack extension.

As the crack tip is approached in a three-dimensional crack, asymptotically the plane-strain or the plane-stress state prevails (Rice, 1968) and therefore we can use the following relationships for the three-dimensional mixed-mode crack:

$$J = J_{\mathrm{I}} + J_{\mathrm{II}} + J_{\mathrm{III}} \tag{16}$$

with

$$J_{\mathrm{I}} = \alpha K_{\mathrm{I}}^2, \qquad J_{\mathrm{II}} = \alpha K_{\mathrm{II}}^2, \qquad J_{\mathrm{III}} = \frac{\alpha}{1-\nu}K_{\mathrm{III}}^2.$$

As in the axisymmetric case, the J integral in Eqs. (15) and (16) alone does not provide adequate information for determining the individual stress intensity factors K_{I}, K_{II} and K_{III} in a mixed-mode crack problem. Other information may be obtained from the two-state J integral (Chen and Shield, 1977). Consider two independent elastic states of a penny-shaped crack in an elastic medium, each denoted by

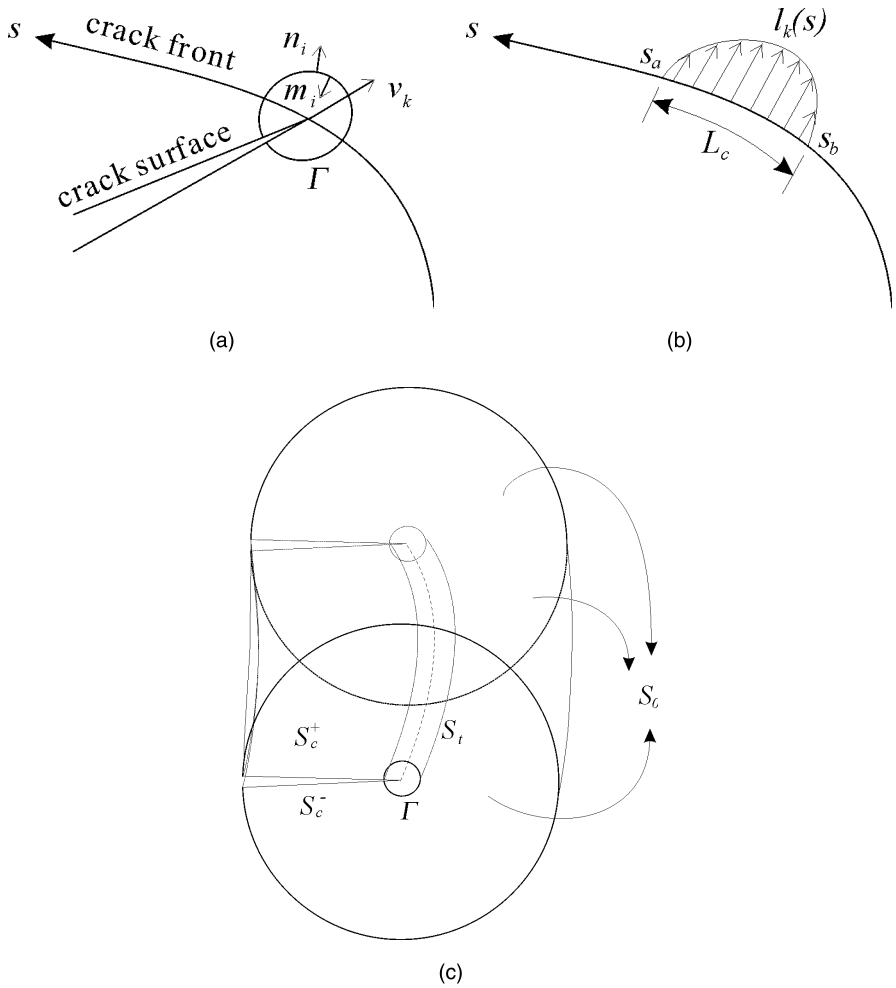

Fig. 2. (a) Conventions at curvilinear crack front (b) virtual crack advance between s_a and s_b (c) inner tubular surface S_t and outer arbitrary surface S_o.

superscript "(1)" and "(2)". Let the equilibrium state from the superposition of the two states be denoted by superscript "(0)". Then the J integral for the superimposed state is obtained in the following form:

$$J^{(0)} = J^{(1)} + J^{(2)} + J^{(1,2)} \tag{17}$$

in which $J^{(k)}$ $(k = 1, 2)$ is defined by Eq. (15), and $J^{(1,2)}$ is given as

$$J^{(1,2)} = -\frac{\lim_{\Gamma \to 0} \int_{S_t} l_k H_{kj}^{(1,2)} m_j \, \mathrm{d}\Gamma}{\int_{L_c} l_k v_k \, \mathrm{d}s} \tag{18}$$

with

$$H_{kj}^{(1,2)} = W^{(1,2)} \delta_{kj} - \left(\sigma_{ij}^{(1)} u_{i,k}^{(2)} + \sigma_{ij}^{(2)} u_{i,k}^{(1)} \right).$$

From Eq. (16), one finds that the J integral for the elastic state "(0)" may be written as

$$J^{(0)} = J^{(1)} + J^{(2)} + 2\alpha\left(K_{\mathrm{I}}^{(1)}K_{\mathrm{I}}^{(2)} + K_{\mathrm{II}}^{(1)}K_{\mathrm{II}}^{(2)} + \frac{1}{1-\nu}K_{\mathrm{III}}^{(1)}K_{\mathrm{III}}^{(2)}\right) \tag{19}$$

and comparison to Eq. (17) yields

$$J^{(1,2)} = 2\alpha\left(K_{\mathrm{I}}^{(1)}K_{\mathrm{I}}^{(2)} + K_{\mathrm{II}}^{(1)}K_{\mathrm{II}}^{(2)} + \frac{1}{1-\nu}K_{\mathrm{III}}^{(1)}K_{\mathrm{III}}^{(2)}\right). \tag{20}$$

Eq. (18) together with Eq. (20) provides, in fact, sufficient information for determining the individual stress intensity factors for a mixed-mode crack when two known auxiliary solutions are introduced. Let two auxiliary solutions be denoted by a superscript "(2*a*)" and "(2*b*)". The auxiliary state "(2*a*)" is chosen to be a pure Mode I state, and "(2*b*)" to be a pure Mode III. Then $J^{(2a)}$ and $J^{(2b)}$ are written as

$$J_{\mathrm{I}}^{(2a)} = \alpha\left[K_{\mathrm{I}}^{(2a)}\right]^2, \qquad J_{\mathrm{III}}^{(2b)} = \alpha\frac{1}{1-\nu}\left[K_{\mathrm{III}}^{(2b)}\right]^2. \tag{21}$$

Together with Eqs. (16) and (20), these lead to the following expression for $K_{\mathrm{I}}^{(1)}$, $K_{\mathrm{II}}^{(1)}$ and $K_{\mathrm{III}}^{(1)}$ in terms of $J^{(1)}$, $J^{(1,2a)}$, $J^{(2a)}$, $J^{(1,2b)}$ and $J^{(2b)}$

$$K_{\mathrm{I}}^{(1)} = \frac{J^{(1,2a)}}{2\sqrt{\alpha J^{(2a)}}} \quad \text{and} \quad J_{\mathrm{I}}^{(1)} = \frac{\left[J_{\mathrm{I}}^{(1,2a)}\right]^2}{4J_{\mathrm{I}}^{(2a)}}, \tag{22}$$

$$K_{\mathrm{III}}^{(1)} = \sqrt{\frac{E}{1+\nu}}\frac{J_{\mathrm{III}}^{(1,2b)}}{2\sqrt{J_{\mathrm{III}}^{(2b)}}} \quad \text{and} \quad J_{\mathrm{III}}^{(1)} = \frac{\left[J_{\mathrm{III}}^{(1,2b)}\right]^2}{4J_{\mathrm{III}}^{(2b)}}, \tag{23}$$

$$K_{\mathrm{II}}^{(1)} = \pm\frac{1}{\sqrt{\alpha}}\sqrt{J^{(1)} - \frac{\left[J_{\mathrm{I}}^{(1,2a)}\right]^2}{4J_{\mathrm{I}}^{(2a)}} - \frac{\left[J_{\mathrm{III}}^{(1,2b)}\right]^2}{4J_{\mathrm{III}}^{(2b)}}} \quad \text{and} \quad J_{\mathrm{II}}^{(1)} = \alpha\left[K_{\mathrm{II}}^{(1)}\right]^2. \tag{24}$$

Note that the path-independent integrals on the right-hand side of the above expressions may be calculated accurately, transforming Eq. (18) into the domain integral expression. The values of $J(s)$ and the two-state integral along a three-dimensional crack front are given by the limiting contour integral as seen in Eqs. (15) and (18). Following Moran and Shih (1987), we can show that the domain integral representation, which is more suitable for numerical computation, is obtained as

$$J(s) = \frac{-\int_V \left(H_{kj}q_{k,j} + H_{kj,j}q_k\right)\mathrm{d}V}{\int_{L_c} l_k(s)v_k(s)\,\mathrm{d}s}, \tag{25}$$

where q_k is the weight function, V is the domain bounded by S_{t} and S_{o} (see Fig. 2c), and L_{c} is the crack front line from s_{a} to s_{b} (see Fig. 2b). It should be noted that S_{t} must shrink onto the crack tip in order to evaluate the pointwise value of J along the crack front. The weight function q_k is smooth enough for the indicated operations to be carried out and is defined as follows

$$q_k = \begin{cases} l_k & \text{on } S_{\mathrm{t}}, \\ 0 & \text{on } S_{\mathrm{o}}, \\ \text{arbitrary} & \text{otherwise.} \end{cases} \tag{26}$$

The divergence term $H_{kj,j}$ in Eq. (25) vanishes if the auxiliary fields satisfy the equilibrium and compatibility in the absence of body force, thermal stress, and inertia.

The success of the present scheme crucially relies upon the availability of the auxiliary solutions. For two-dimensional crack problems, we see that the three modes of the **K**-fields, which have inverse square root singularity, are valid over the entire domain, and therefore they naturally come up as a set of three independent auxiliary solutions. However, there exist no simple auxiliary solutions available for three-dimensional cracks with a curved line of crack front or tip. In spite of such a limitation, however, the present scheme is applicable for three-dimensional cracks once we have any auxiliary solution valid only on the local region where the domain integral is carried out. For such auxiliary solutions, we may therefore choose the solutions for an axisymmetric penny-shaped crack with the same radius as the radius of curvature of the local crack front line in the target problem of a three-dimensional crack for which we want to decompose the fracture modes. The solution for a penny-shaped crack in an infinite body is given in the integral form (Hartranft and Sih, 1973; Kassir and Sih, 1974) and so not convenient for numerical computation.

In order to obtain auxiliary fields, we take finite element solutions to penny-shaped crack problems under pure Mode I and Mode III. We demonstrate in the next section the validity of the numerical auxiliary fields through some numerical examples. Another choice of auxiliary field is the use of the plane-strain asymptotic solution. Away from a curved crack front the plane-strain asymptotic solution fails to meet the equilibrium and the compatibility, and so arises nonzero divergence term $H_{kj,j}$ in Eq. (25) for a curved three-dimensional crack. In general, this divergence term should be included in the calculation of the two-state integral to decompose the mixed modes in a curved three-dimensional crack, because the auxiliary fields in the form of the asymptotic plane-strain solution or **K**-field do not satisfy the equilibrium and compatibility in three-dimensional domain with curved cracks. In other words, the three-dimensional effect should be considered with the divergence term retained in the two-state integral. In particular, it is crucial to incorporate the divergence term in the two-state integral for a highly curved crack. The divergence term in the two-state integral can be written as

$$H_{kj,j}^{(1,2)} = \sigma_{ij}^{(1)}\varepsilon_{ij,k}^{(2)} - \sigma_{ij}^{(1)}u_{i,kj}^{(2)} - \sigma_{ij,j}^{(2)}u_{i,k}^{(1)} \tag{27}$$

in which superscript (2) indicates an auxiliary field. The higher order gradients in Eq. (27) give rise to the difficulty in evaluating the divergence term. Nahta and Moran (1993) and Gosz et al. (1998) presented a method to evaluate the divergence term by introducing curvilinear coordinates in the expression of deformation gradients. In this paper, we propose a simple method to impose the plane-strain asymptotic solutions, as auxiliary fields, on three-dimensional domain. The displacements of two-dimensional asymptotic solution are imposed on the nodes of three-dimensional finite element model, and then the first and second terms in Eq. (27) cancel each other because displacement field satisfies compatibility condition; i.e., $\sigma_{ij}^{(1)}\varepsilon_{ij,k}^{(2)} = \sigma_{ij}^{(1)}u_{i,kj}^{(2)}$. In the present method, the stresses of the asymptotic solutions are used in the expression of the two-state integral, and the strains are evaluated at the integration points by using finite element interpolation from the nodal values of the two-dimensional asymptotic solution. The equilibrium equation in the absent of body force in the cylindrical coordinates shown in Fig. 3 can be reduced to the following forms:

$$r\text{-direction} \quad \left[\frac{\partial\sigma_{rr}^{(2)}}{\partial r} + \frac{1}{\rho}\frac{\partial\sigma_{r\theta}^{(2)}}{\partial\theta} + \frac{\partial\sigma_{rz}^{(2)}}{\partial z}\right] + \frac{\sigma_{rr}^{(2)} - \sigma_{\theta\theta}^{(2)}}{\rho} = \frac{\sigma_{rr}^{(2)} - \sigma_{\theta\theta}^{(2)}}{\rho}, \tag{28a}$$

$$\theta\text{-direction} \quad \left[\frac{\partial\sigma_{r\theta}^{(2)}}{\partial r} + \frac{1}{\rho}\frac{\partial\sigma_{\theta\theta}^{(2)}}{\partial\theta} + \frac{\partial\sigma_{\theta z}^{(2)}}{\partial z}\right] + 2\frac{\sigma_{r\theta}^{(2)}}{\rho} = 2\frac{\sigma_{r\theta}^{(2)}}{\rho}, \tag{28b}$$

$$z\text{-direction} \quad \left[\frac{\partial\sigma_{rz}^{(2)}}{\partial r} + \frac{1}{\rho}\frac{\partial\sigma_{\theta z}^{(2)}}{\partial\theta} + \frac{\partial\sigma_{zz}^{(2)}}{\partial z}\right] + \frac{\sigma_{rz}^{(2)}}{\rho} = \frac{\sigma_{rz}^{(2)}}{\rho}, \tag{28c}$$

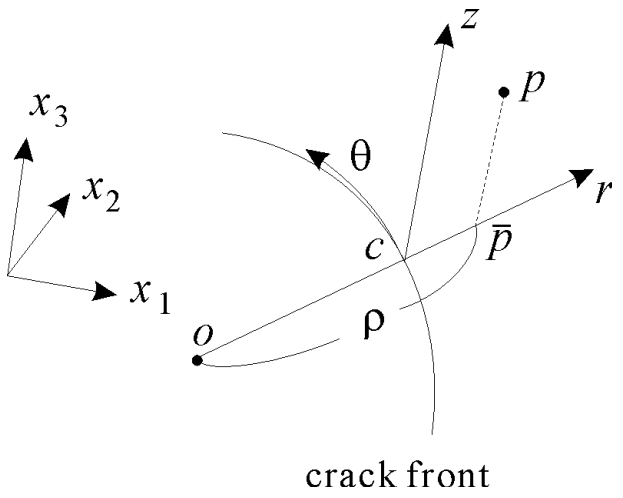

Fig. 3. Local cylindrical coordinates on the crack front; $\bar{p}$ is the projection point of p on the plane parallel to the crack surface.

where ρ is the radius on the plane parallel to the crack surface as shown in Fig. 3. In this figure, the line $p\bar{p}$ is perpendicular to the plane of crack surface, and the cylindrical coordinates are defined at the point c lying on the crack front. The expressions inside bracket in Eqs. (28a)–(28c) indicate the equilibrium for the asymptotic solution in two-dimensional domain. Consequently, the divergence term in the present method can be written as

$$H^{(1,2)}_{kj,j} = -\sigma^{(2)}_{ij,j}u^{(1)}_{i,k} = -\begin{bmatrix} u^{(1)}_{1,k} & u^{(1)}_{2,k} & u^{(1)}_{3,k} \end{bmatrix} \begin{bmatrix} \mathbf{e}_1\cdot\mathbf{e}_r & \mathbf{e}_1\cdot\mathbf{e}_\theta & \mathbf{e}_1\cdot\mathbf{e}_z \\ \mathbf{e}_2\cdot\mathbf{e}_r & \mathbf{e}_2\cdot\mathbf{e}_\theta & \mathbf{e}_2\cdot\mathbf{e}_z \\ \mathbf{e}_3\cdot\mathbf{e}_r & \mathbf{e}_3\cdot\mathbf{e}_\theta & \mathbf{e}_3\cdot\mathbf{e}_z \end{bmatrix} \begin{Bmatrix} \left(\sigma^{(2)}_{rr} - \sigma^{(2)}_{\theta\theta}\right)/\rho \\ 2\sigma^{(2)}_{r\theta}/\rho \\ \sigma^{(2)}_{rz}/\rho \end{Bmatrix}, \tag{29}$$

where the basis vectors $(\mathbf{e}_1, \mathbf{e}_2, \mathbf{e}_3)$ and $(\mathbf{e}_r, \mathbf{e}_\theta, \mathbf{e}_z)$ in (x_1, x_2, x_3) and (r, θ, z) coordinates, respectively, are introduced for coordinate transformation. For example, we have the following expression for the divergence term in the two-state integral when the crack surface lies in the x_1–x_2 plane:

$$H^{(1,2)}_{kj,j} = -\left(\frac{\sigma^{(2)}_{rr} - \sigma^{(2)}_{\theta\theta}}{\rho}\cos\theta - \frac{2\sigma^{(2)}_{r\theta}}{\rho}\sin\theta\right)u^{(1)}_{1,k} - \left(\frac{\sigma^{(2)}_{rr} - \sigma^{(2)}_{\theta\theta}}{\rho}\sin\theta + \frac{2\sigma^{(2)}_{r\theta}}{\rho}\cos\theta\right)u^{(1)}_{2,k} - \frac{\sigma^{(2)}_{rz}}{\rho}u^{(1)}_{3,k}, \tag{30}$$

where θ is the angle between x_1 axis and r axis in the x_1–x_2 plane. It should be emphasized that the expression (29) or (30) is easily calculated from the stresses $(\sigma_{rr}, \sigma_{\theta\theta}, \sigma_{r\theta}, \sigma_{rz})$ of the plane-strain asymptotic field.

3. Finite element implementation

3.1. Axisymmetric finite element implementation

In the foregoing we have established the mode decomposition method for axisymmetric and three-dimensional cracks under mixed mode loading. Accuracy of the method described in Section 2 depends on how accurately the conservation integrals are evaluated. The integration path may be chosen along the

element boundaries or through the Gaussian points. Li et al. (1985), Nikishkov and Atluri (1987b), and Shih and Asaro (1988) have introduced appropriate weighting functions to obtain area/domain representation of the J integral. They concluded that a very accurate value of J is obtained using the domain representation and the value of J so obtained is insensitive to the types of weighting function. In an analogous manner it is possible to recast the line integral J of Eqs. (5a) and (5b) into the area integral:

$$J = \frac{1}{r_c^2} \int_{A_1} F_m x_1 \frac{\partial q}{\partial x_m} \, dA, \tag{31}$$

where A_1 is an area enclosed by C_1 and C_2 as shown in Fig. 1 and the function F_m is given in Eqs. (5a) and (5b). Moreover, q is a weight function which has the value of zero on the contour C_2 and one on the inner contour C_1. Use is made of the equilibrium equation and divergence theorem in deriving the expression (31).

3.2. Three-dimensional finite element implementation

In a three-dimensional analysis the virtual crack extension has to be applied to a single node point on the crack front for evaluating the local value of the energy release rate. For the 20-node three-dimensional isoparametric element, a new crack front is defined by the quadratic interpolation function as shown in Fig. 4. The volume V is identified with the collection of elements which contain the line L_c. Thus, in the finite element framework, for considering the increase in cracked area due to the shift of a given particular node M we take L_c to be the line connecting the nodes $M-1$, M and $M+1$ for mid nodes and the nodes $M-2$, $M-1$, M, $M+1$ and $M+2$ for corner nodes as shown in Fig. 4. Then, the weight function is therefore taken as follows (Li et al., 1985)

$$q_i = \sum_{k=1}^{20} N^k Q^k, \tag{32}$$

where N^k is the triquadratic shape function and Q^k is the nodal values for the kth node. Note that $Q^k = 0$ if the kth node is on S_o. For nodes inside V, Q^k is given by interpolation between the nodal values on L_c and S_o (see Fig. 2).

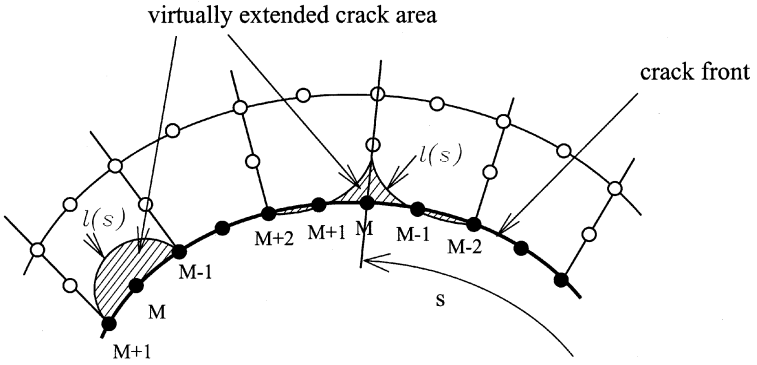

Fig. 4. Local advance of the crack front for 20-noded three-dimensional element.

4. Numerical examples and discussion

The procedures just outlined have been programmed for studying axisymmetric penny-shaped cracks and three-dimensional cracks under mixed mode loading in isotropic solids. The numerical calculations for mixed-mode crack problems are carried out with the finite element code ABAQUS (Hibbitt et al., 1997). This code supplies the required displacements and stresses at the Gaussian points to a separate program developed for evaluating the J integral and the two-state integrals. For the convenience of the notation, we use x, y, and z in the numerical experiments instead of x_1, x_2 and x_3 in the previous sections, respectively.

4.1. An axisymmetric sub-interface penny-shaped crack

To illustrate the decomposition method for axisymmetric mixed-mode cracks, an axisymmetric sub-interface penny-shaped crack is selected as an example problem. The problem of a straight crack paralleling an interface between two dissimilar materials has attracted a substantial amount of attention due to its potential application in various kinds of bonding problems (Hutchinson et al., 1987; Yang and Kim, 1993).

In this paper the problem of a penny-shaped crack paralleling an interface between two dissimilar materials under tension is investigated. The loading condition and the crack geometry under investigation are shown in Fig. 5a ($\sigma_t = 6.895 \times 10^5$ N/m^2). The cylinder has a radius $b = 0.0572$ m; total length of $2L = 0.127$ m. The penny-shaped crack has a radius $a = 0.0254$ m ($a/b = 0.444$); a distance from the interface to the penny-shaped crack is $h = 0.00635$ m. Each material is taken to be isotropic and elastic. The upper part of the cylinder has elastic properties of $E_1 = 2.069 \times 10^9$ N/m^2 and $\nu_1 = 0.3$. The lower part containing a penny-shaped crack has elastic properties of $E_2 = 2.069 \times 10^{11}$ N/m^2 and $\nu_2 = 0.3$.

To examine the accuracy and the convergence of the results, a typical finite element mesh for a penny-shaped crack paralleling an interface between two dissimilar materials is selected as shown in Fig. 5b wherein a total of 298 eight-noded isoparametric-axisymmetric elements are used. To find a Mode I auxiliary field, we consider a body of the same geometry as in the target problem, but composed of the lower material ($E = E_2$ and $\nu = \nu_2$) only. Because the body is made of a homogeneous material, it will undergo a pure Mode I deformation under a remote tension $\sigma_t = 6.895 \times 10^5$ N/m^2. Note that the foregoing mode

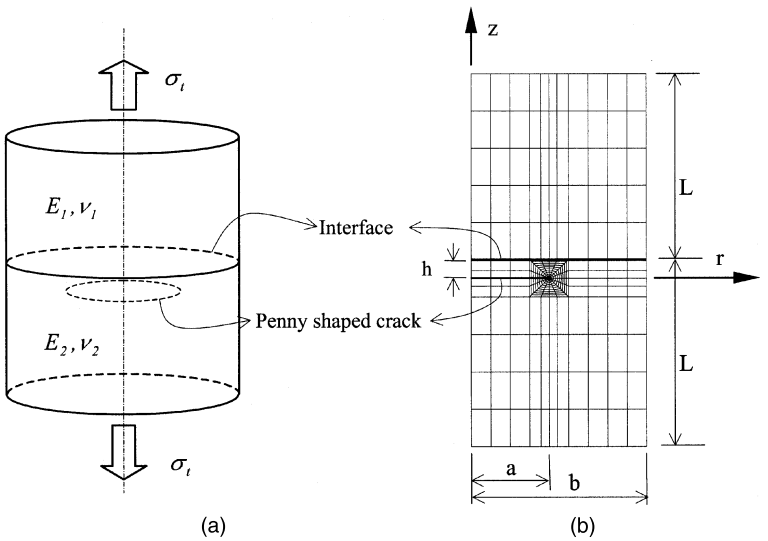

Fig. 5. (a) Axisymmetric sub-interface penny-shaped crack (b) finite element model for axisymmetric sub-interface penny-shaped crack.

decomposition scheme is applicable only when an auxiliary field is found for the target problem, i.e. the geometry and the material properties should coincide between the auxiliary field and the target problem. Hence we restrict our attention to the lower part of the target field, which has the same geometry and properties as the auxiliary field. This is equivalent to removing the upper part and applying the external traction, which is acting upon the lower material by the upper one, so that the mode decomposition scheme is now applied on the lower part of the body. It is under a mixed mode in the target problem while it is under pure Mode I in the auxiliary field. The first integration domain is comprised of 16 elements adjoining the crack tip; the second domain has the next 16 elements adjoining the first integration domain. In this manner, the integration domains 3 through 9 are continued. The detailed element arrangement around the crack tip and the domains selected for integration are given in Fig. 6 wherein the paths of the integration domains 3 and 7 are indicated. The calculations for J integrals are carried out according to the domain integral (31) in a separate post-processing program, and the two-state integrals are calculated in the same manner.

The path independence of J and two-state integral has been checked numerically by using different domains of integration. The values of J and two-state integral as calculated by the discrete domain formula of the type of Eq. (31) for the various domains are listed in Table 1. We observe that the variation in the computed J and two-state integral from one domain to another is within 1% excluding the near tip domain of the first domain. Effects of E_1/E_2 are examined by taking various material constant E_1 or E_1/E_2 for the given lower part containing a penny-shaped crack and $v_1 = v_2 = 0.3$. A plot of the variation of the computed K_I and K_{II} with the increase of E_1/E_2 is shown in Fig. 7. This shows well the mixed mode of the sub-interface penny-shaped crack even under uniaxial tension loading, because K_I and K_{II} are of the same order of magnitude. It is noticed that K_I is always higher than K_{II} in the entire range of E_1/E_2 examined. In the case of $E_1/E_2 < 1$, K_I and K_{II} increase as E_1/E_2 decreases. K_I and K_{II} remain relatively unchanged with E_1/E_2 greater than 30. Note that K_{II} disappears for $E_1/E_2 = 1$. This K_I is found to be $K_I = 1.2089\sigma_t\sqrt{a}$, and

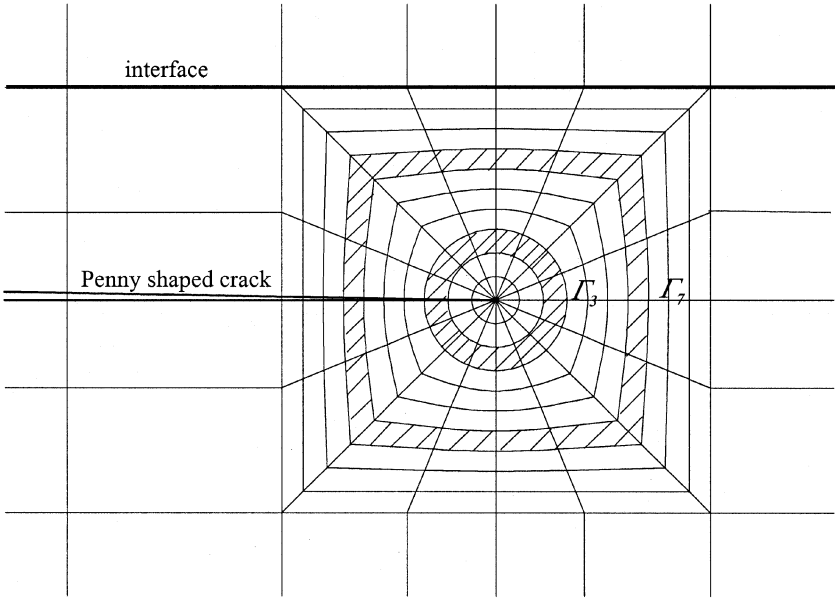

Fig. 6. The detailed element arrangement around the crack tip and the paths of the integration domains.

Table 1
Axisymmetric analysis result for a sub-interface penny-shaped crack

Domain	$J^{(1)}$ (Pa m)	$J^{(1,2)}$ (Pa m)	$J^{(2)}$ (Pa m)	K_I (kPa m$^{1/2}$)	K_{II} (kPa m$^{1/2}$)
1	4.0466E − 01	3.2799E − 01	7.6300E − 02	2.8305E + 02	1.0892E + 02
2	4.1197E − 01	3.3347E − 01	7.7558E − 02	2.8544E + 02	1.1032E + 02
3	4.1235E − 01	3.3307E − 01	7.7640E − 02	2.8496E + 02	1.1194E + 02
4	4.1240E − 01	3.3312E − 01	7.7645E − 02	2.8499E + 02	1.1191E + 02
5	4.1242E − 01	3.3314E − 01	7.7645E − 02	2.8501E + 02	1.1189E + 02
6	4.1244E − 01	3.3316E − 01	7.7643E − 02	2.8502E + 02	1.1188E + 02
7	4.1246E − 01	3.3316E − 01	7.7643E − 02	2.8502E + 02	1.1188E + 02
8	4.1246E − 01	3.3316E − 01	7.7643E − 02	2.8502E + 02	1.1189E + 02
9	4.1244E − 01	3.3316E − 01	7.7642E − 02	2.8502E + 02	1.1187E + 02
Average excluding the first domain					
	4.1237E − 01	3.3317E − 01	7.7642E − 02	2.8496E + 02	1.1170E + 02

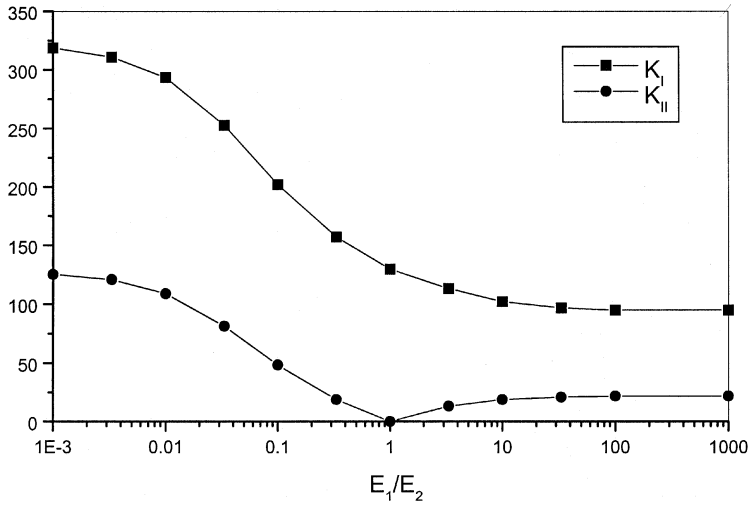

Fig. 7. The variation of K_I and K_{II} with the increase of $E_1/E_2(\nu_1 = \nu_2 = 0.3)$.

this is well compared with $K_I = 1.1903\sigma_t\sqrt{a}$ for an axisymmetric crack in an infinite homogeneous body from Benthem and Koiter (1973).

4.2. Three-dimensional penny-shaped crack under nonaxisymmetric loading

We first compare the results from the decomposition method for three-dimensional mixed-mode cracks with those for the axisymmetric mixed mode crack in Section 4.1. We consider the full three-dimensional model consisting of a 360° revolution of the same axisymmetric model as in the previous section about the z axis. The model is discretized with 10 elements along the circumference in an 180° segment. The typical finite element mesh for the full three-dimensional model is similar to that illustrated in Fig. 8. A total of 5740 20-noded isoparametric elements are used. The elements adjoining the crack front are set to possess the inverse square root singularity at the corner nodes on the crack tip by choosing the mid nodes to be located on the quarter point.

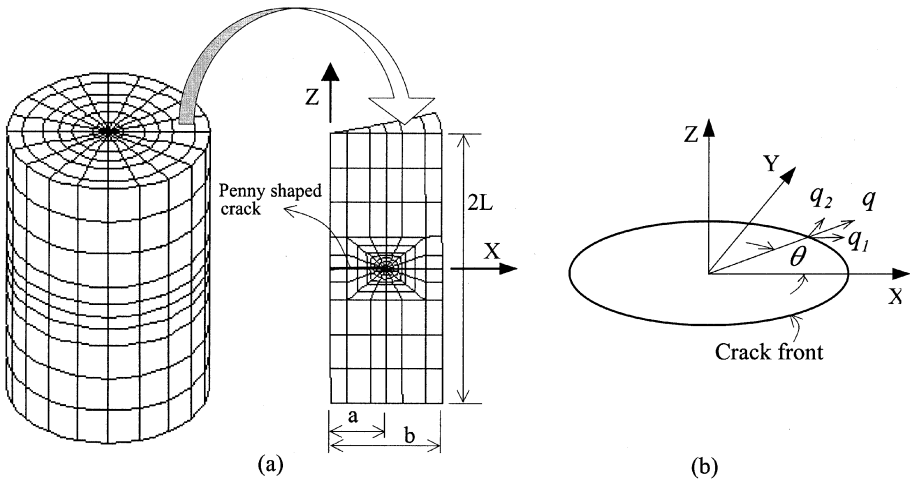

Fig. 8. (a) Three-dimensional finite element model for the penny-shaped crack under nonaxisymmetric loading (b) the definition of q_i along the penny-shaped crack.

We briefly discuss the setting up of the integration domains for calculating J and two-state integrals associated with a unit virtual advance of a finite crack front segment (e.g. see Fig. 8). The first integration domain is comprised of a collection of elements adjoining the crack front: the domain consists of two layers of elements in the circumferential direction, amounting to a total of 32 elements, for a unit virtual advance of a corner node, while it contains only one layer of elements or a total of 16 elements if a unit virtual advance is imposed on a mid node. The second domain is obtained by adding one ring of elements around the first domain; thus the second domain has a total of 64 elements for a virtual advance of a corner node and a total of 32 elements for a virtual advance of a mid node. In this manner, the integration domains 3 through 9 are continued.

The loading condition and the crack geometry under investigation are the same as those in the previous part ($E_1 = 2.069 \times 10^9$ N/m^2, $E_2 = 2.069 \times 10^{11}$ N/m^2 and $v_1 = v_2 = 0.3$). As an auxiliary solution, Mode I loading condition was used for the cylinder of a homogeneous material $E_1 = E_2 = 2.069 \times 10^{11}$ N/m^2. The results for three-dimensional mixed-mode crack are shown in Table 2. It is seen from this table that the J and the two-state integral are path-independent except the first domain. In Table 3, they are compared with the results from the axisymmetric analysis of the foregoing section. Comparison of the results shows that the three-dimensional solution is in an excellent agreement with the axisymmetric solution. Particularly, the path independence in different annular regions containing crack front at its center for domain integrals indicates the minor effects of boundary. In the three-dimensional solution the J and the two-state integral for a virtual advance of a corner node differ only slightly from those for a virtual advance of a mid node.

To illustrate the mode separation for three-dimensional mixed-mode cracks, selected are two examples of a circular cylinder containing a penny-shaped crack and a half-circular cylinder containing a half-penny-shaped surface crack at its center under nonaxisymmetric loading. The crack geometry and the finite element mesh are shown in Fig. 8. The cylinder has a radius $b = 0.0508$ m; total length of $2L = 0.152$ m. The penny-shaped crack has a radius $a = 0.0254$ m ($a/b = 0.5$). For auxiliary solutions, two different loadings are chosen; one is a uniform tension, generating a pure Mode I deformation, and the other a torsion, giving rise to a pure Mode III. To apply nonaxisymmetric loading, the lower end face of the circular cylinder at $z = -L$ is constrained against motion in the x, y and z, whereas the uniform displacement boundary condition of $u_x = 2.54 \times 10^{-6}$ m and $u_z = 7.62 \times 10^{-7}$ m are applied on the other end face of the circular cylinder at $z = L$ (Fig. 8).

Table 2
Three-dimensional analysis results for a sub-interface penny-shaped crack

Domain	$J^{(1)}$ (Pa m)	$J^{(1,2)}$ (Pa m)	$J^{(2)}$ (Pa m)	K_I (kPa m$^{1/2}$)	K_{II} (kPa m$^{1/2}$)
Corner node					
1	4.2172E − 01	3.4032E − 01	7.9547E − 02	2.8765E + 02	1.1455E + 02
2	4.1729E − 01	3.3676E − 01	7.8715E − 02	2.8613E + 02	1.1393E + 02
3	4.1624E − 01	3.3592E − 01	7.8521E − 02	2.8578E + 02	1.1379E + 02
4	4.1584E − 01	3.3559E − 01	7.8444E − 02	2.8564E + 02	1.1374E + 02
5	4.1559E − 01	3.3540E − 01	7.8398E − 02	2.8549E + 02	1.1368E + 02
6	4.1542E − 01	3.3526E − 01	7.8369E − 02	2.8549E + 02	1.1368E + 02
7	4.1531E − 01	3.3517E − 01	7.8347E − 02	2.8546E + 02	1.1366E + 02
8	4.1522E − 01	3.3512E − 01	7.8332E − 02	2.8544E + 02	1.1364E + 02
9	4.1514E − 01	3.3506E − 01	7.8321E − 02	2.8542E + 02	1.1359E + 02
Average excluding the first domain					
	4.1575E − 01	3.3554E − 01	7.8432E − 02	2.8562E + 02	1.1371E + 02
Mid node					
1	4.1673E − 01	3.3631E − 01	7.8610E − 02	2.8594E + 02	1.1385E + 02
2	4.1230E − 01	3.3274E − 01	7.7777E − 02	2.8442E + 02	1.1324E + 02
3	4.1125E − 01	3.3189E − 01	7.7580E − 02	2.8407E + 02	1.1311E + 02
4	4.1083E − 01	3.3156E − 01	7.7502E − 02	2.8391E + 02	1.1305E + 02
5	4.1058E − 01	3.3135E − 01	7.7454E − 02	2.8382E + 02	1.1301E + 02
6	4.1042E − 01	3.3123E − 01	7.7425E − 02	2.8377E + 02	1.1299E + 02
7	4.1030E − 01	3.3114E − 01	7.7404E − 02	2.8374E + 02	1.1297E + 02
8	4.1021E − 01	3.3107E − 01	7.7388E − 02	2.8371E + 02	1.1294E + 02
9	4.1013E − 01	3.3104E − 01	7.7377E − 02	2.8369E + 02	1.1290E + 02
Average excluding the first domain					
	4.1076E − 01	3.3151E − 01	7.7488E − 02	2.8389E + 02	1.1302E + 02

Table 3
Comparison between the axisymmetric analysis result and the three-dimensional analysis results

Analysis	$J^{(1)}$ (Pa m)	$J^{(1,2)}$ (Pa m)	$J^{(2)}$ (Pa m)	K_I (kPa m$^{1/2}$)	K_{II} (kPa m$^{1/2}$)
Axisymmetric					
Average	4.1237E − 01	3.3317E − 01	7.7642E − 02	2.8496E + 02	1.1170E + 02
Three dimensional					
Corner node	4.1575E − 01	3.3554E − 01	7.8432E − 02	2.8562E + 02	1.1371E + 02
Mid node	4.1076E − 01	3.3151E − 01	7.7488E − 02	2.8389E + 02	1.1302E + 02
Average	4.1326E − 01	3.3352E − 01	7.7960E − 02	2.8476E + 02	1.1337E + 02
Maximum relative difference from axisymmetric analysis result[a]					
	0.8	0.5	1.0	0.4	1.8

[a] $(\max|a-b|/a) \times 100$; a: axisymmetric analysis result; b: three-dimensional analysis result (corner node of mid node result).

The solution procedure starts from the choice of the independent auxiliary fields, which are obtained by the choice of the two different loadings – uniform tension and torsion. For the auxiliary field of Mode I, the same finite element model as that for the target field is used under tension with $\sigma_t = 6.895 \times 10^5$ N/m^2, and for the auxiliary field of Mode III the same finite element model under torsion with the applied torque of 4.61 kg m. With both of the auxiliary field data and the target field data from ABAQUS output file the evaluation of the J and two-state integral is carried out for the domain selected as described in this section.

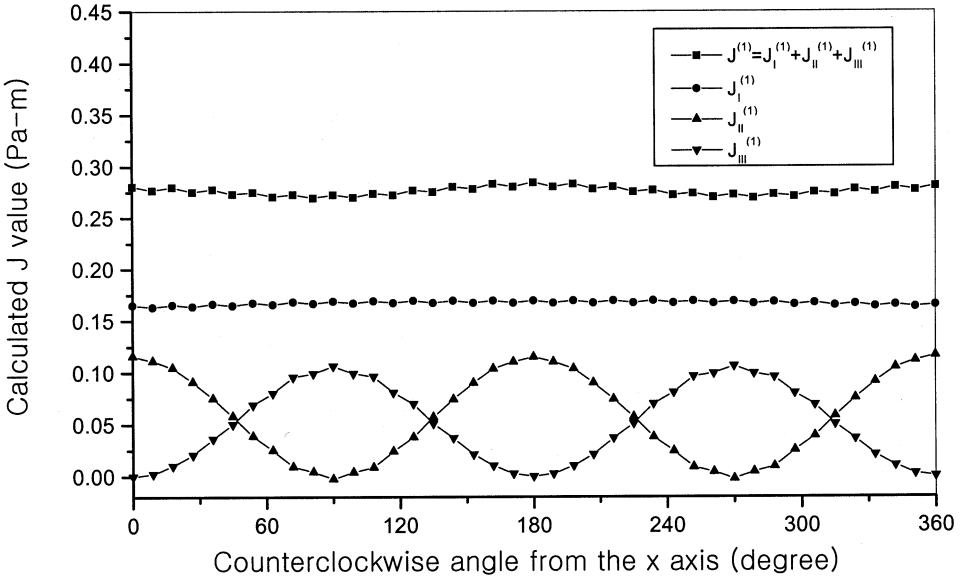

Fig. 9. The calculated pointwise values of $J^{(1)}$, $J_{\mathrm{I}}^{(1)}$, $J_{\mathrm{II}}^{(1)}$ and $J_{\mathrm{III}}^{(1)}$ along the crack front of the penny-shaped crack.

A plot of the variation of the computed $J^{(1)}$, $J_{\mathrm{I}}^{(1)}$, $J_{\mathrm{II}}^{(1)}$ and $J_{\mathrm{III}}^{(1)}$ along the crack front of the penny-shaped crack is shown in Fig. 9. In the plot, $J^{(1)}$ at the intersection of the crack boundary with the x axis is slightly greater than that at the intersection of the crack boundary with the y axis. $J_{\mathrm{I}}^{(1)}$ is constant along the crack front of the penny-shaped crack as expected. Note that $J_{\mathrm{II}}^{(1)}$ and $J_{\mathrm{III}}^{(1)}$ vary like the curves for the squares of $\cos\theta$ and $\sin\theta$ along the crack front line of the penny-shaped crack. It is noticed that $J_{\mathrm{II}}^{(1)}$ is greatest at the intersection of the crack boundary with the x axis and vanishes at the intersection of the crack boundary with the y axis. On the other hand, $J_{\mathrm{III}}^{(1)}$ vanishes at the intersection of the crack boundary with the x axis and is greatest at the intersection of the crack boundary with the y axis. This is consistent with the applied displacements of u_x and u_z on the top face of the cylinder.

With these values of J and the two-state integrals, K_{I}, K_{II} and K_{III} are obtained from Eqs. (22)–(24). A plot of the variation of the computed K_{I}, K_{II} and K_{III} along the crack front is shown in Fig. 10, in which the absolute values of the stress intensity factors neglecting sign change are plotted. Note that K_{I} is constant along the crack front line of the penny-shaped crack. As expected, K_{II} and K_{III} vary like curves of $\cos\theta$ and $\sin\theta$ respectively along the crack front line of the penny-shaped crack. Each of the stress intensity factors K_{I}, K_{II} and K_{III} have the variation consistent with that of each of $J_{\mathrm{I}}^{(1)}$, $J_{\mathrm{II}}^{(1)}$ and $J_{\mathrm{III}}^{(1)}$ along the circumferential direction.

The crack geometry and the finite element mesh for the second example are shown in Fig. 11. The half-circular cylinder has a radius $b = 0.0508$ m; total length of $2L = 0.152$ m. The half-penny-shaped surface crack has a radius $a = 0.0254$ m ($a/b = 0.5$), which is of the same size as in the foregoing example. For auxiliary solutions, the same auxiliary field solutions as in the previous example are used.

To apply nonaxisymmetric loading, the lower end face of the half-circular cylinder at $z = -L$ is constrained against motion in x, y and z, whereas the same uniform displacement boundary condition of $u_x = 2.54 \times 10^{-6}$ m and $u_z = 7.62 \times 10^{-7}$ m as in the previous example are applied on the other end face of the half-circular cylinder at $z = L$.

A plot of the variation of the computed $J^{(1)}$, $J_{\mathrm{I}}^{(1)}$, $J_{\mathrm{II}}^{(1)}$ and $J_{\mathrm{III}}^{(1)}$ along the crack front of the half-penny-shaped surface crack is shown in Fig. 12. In the plot, $J^{(1)}$, $J_{\mathrm{I}}^{(1)}$ and $J_{\mathrm{II}}^{(1)}$ at the surface are greater than those

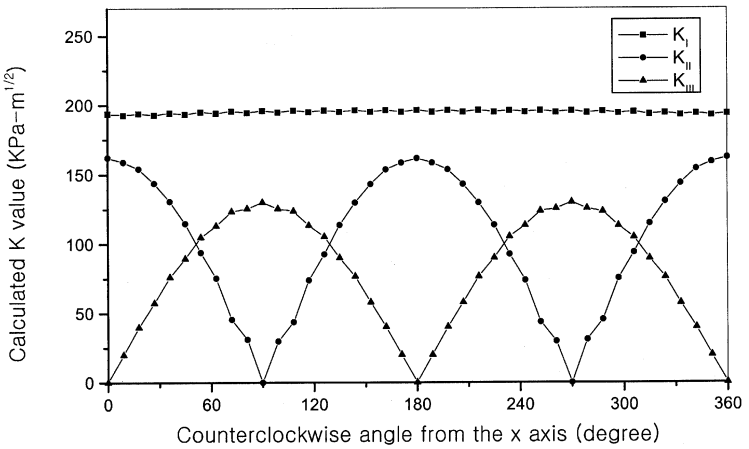

Fig. 10. The variation of the computed K_{I}, K_{II} and K_{III} along the crack front of the penny-shaped crack.

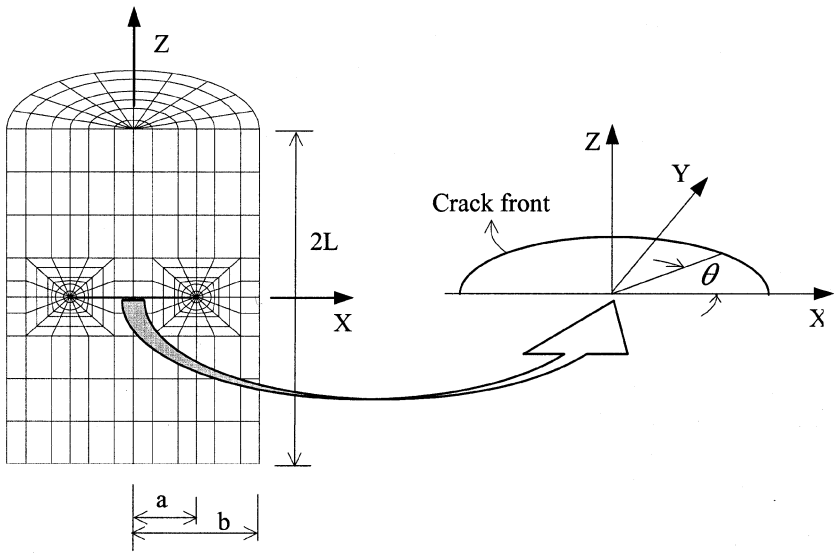

Fig. 11. Three-dimensional finite element model for half-penny-shaped surface crack under nonaxisymmetric loading.

at the deepest interior point of the crack front, which is consistent with the numerical and experimental results obtained by Ernst et al. (1994) and Sharobeam and Landes (1995). A plot of the variation of the computed K_{I}, K_{II} and K_{III} along the crack front is shown in Fig. 13. Note that K_{I} and K_{II} at the surface are greater than those at the deepest interior point of the crack front. As expected, K_{II} and K_{III} vary like the curves of $\cos\theta$ and $\sin\theta$, respectively along the crack front line of the half-penny-shaped surface crack.

4.3. Mode decomposition using plane-strain asymptotic auxiliary fields

Next, we consider the mode decomposition using auxiliary fields of the asymptotic solutions for the plane problems. Nahta and Moran (1993) and Gosz et al. (1998) have used the asymptotic auxiliary fields to

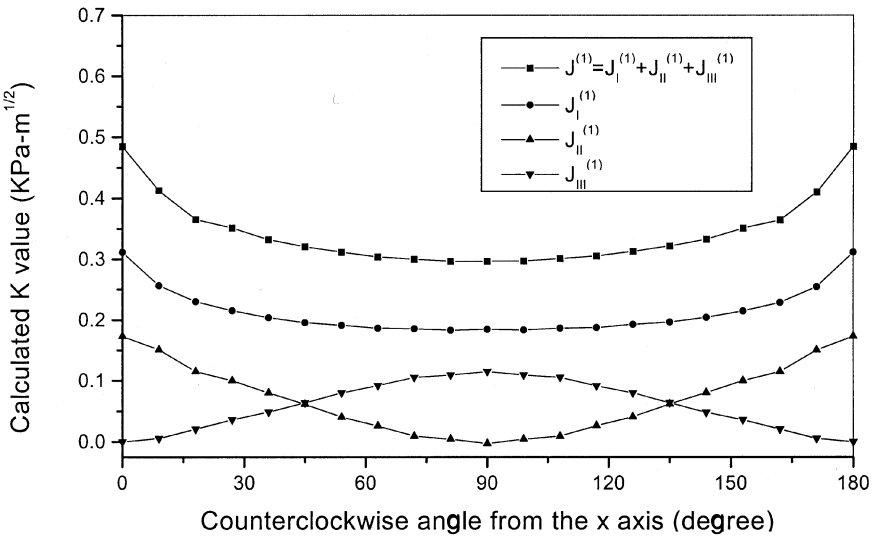

Fig. 12. The calculated pointwise values of $J^{(1)}$, $J_{\mathrm{I}}^{(1)}$, $J_{\mathrm{II}}^{(1)}$ and $J_{\mathrm{III}}^{(1)}$ along the crack front of the half-penny-shaped surface crack.

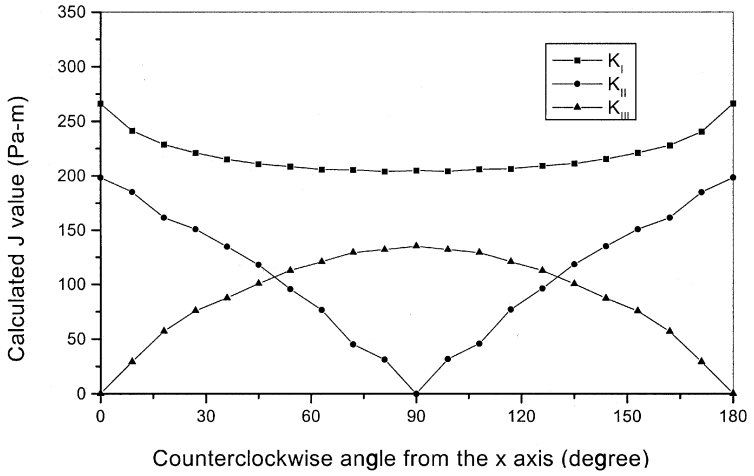

Fig. 13. The variation of the computed K_{I}, K_{II} and K_{III} along the crack front of the half-penny-shaped surface crack.

determine the stress intensity factors for three-dimensional mixed-mode cracks. In their works, they presented a method to evaluate the divergence term in the two-state integral with the aid of deformation gradients using curvilinear coordinates. In this paper, we proposed a simple method to calculate the two-state integral through imposing displacements of the two-dimensional asymptotic solutions on the nodes in finite element models. As explained before, the divergence term can be easily evaluated with a simple form (29) or (30). The penny-shaped crack embedded in a cylinder under mixed mode is adopted to study the mode decomposition using asymptotic auxiliary fields. We take the same material and geometry as those in the previous part ($E = 2.069 \times 10^{11}$ N/m^2, $v = 0.3$, $a = 0.0254$ m, $b = 0.0508$ m). The bottom surface is fixed not to move in any direction, and the displacements $u_x = 2.54 \times 10^{-6}$ m and $u_z = 7.62 \times 10^{-7}$ m are

applied on the top surface. As a reference solution to verify the effectiveness of the present method, the mode decomposition using numerical auxiliary solutions under pure Mode I and Mode III, which is described in the previous part, is carried out for two types of finite element models – the first model with seven rings along the crack front as shown in Fig. 8, and the second model with four rings along the crack front as shown in Fig. 14. The stress intensity factors versus the angle from the x axis, using numerical auxiliary fields for these two finite element models, are plotted in Fig. 15. In this figure, we distinguish the sign change of the stress intensity factors. Since the results for the models with different mesh sizes show a good agreement with each other, the stress intensity factors obtained using numerical auxiliary fields are taken as reference solution to compare with the results obtained using the asymptotic auxiliary fields. Moreover, we have demonstrated the validity of the numerical auxiliary fields in the previous parts. In the comparison,

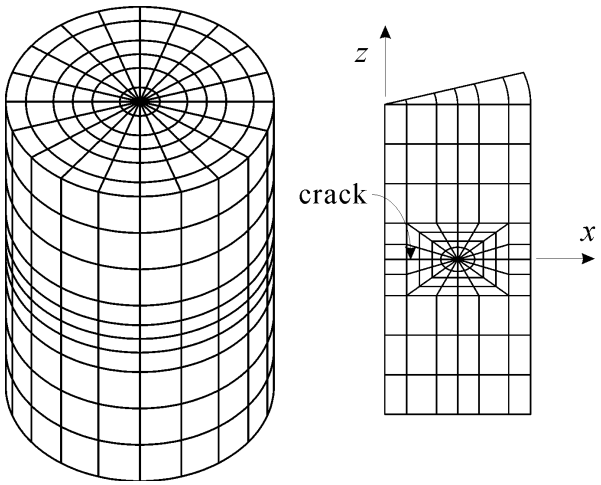

Fig. 14. Three-dimensional finite element model with four rings along the crack front.

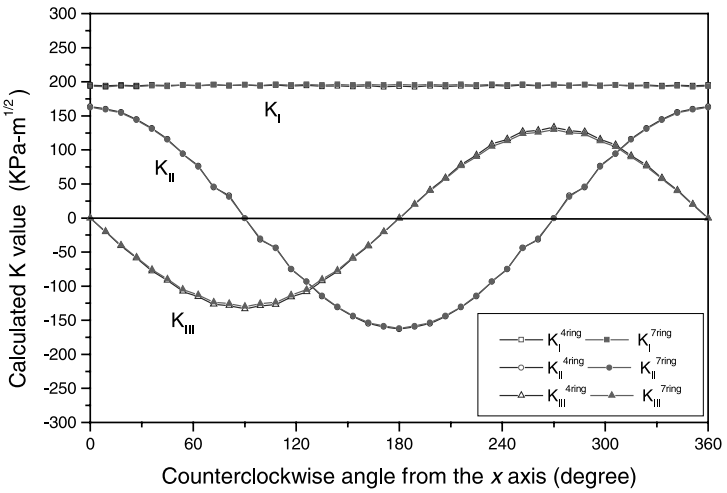

Fig. 15. Comparison of stress intensity factors calculated by using numerical auxiliary fields for two types of meshes with four rings and with seven rings.

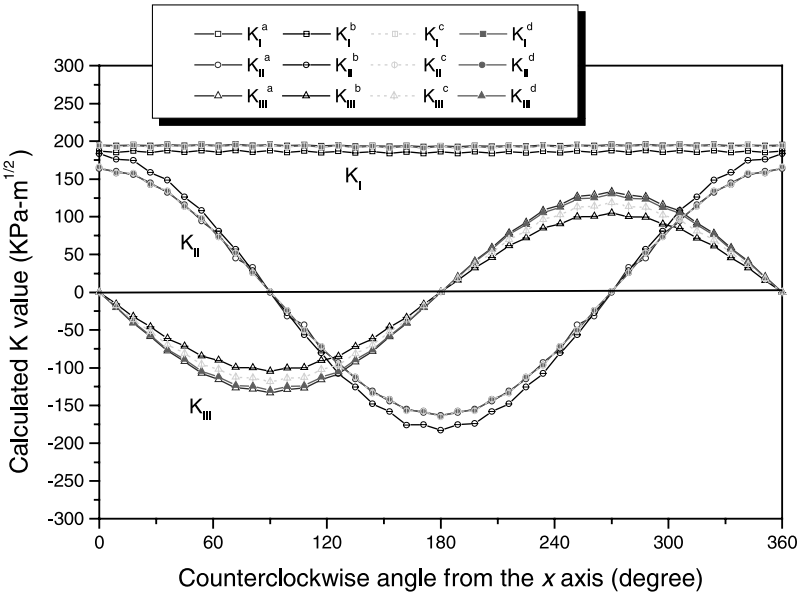

Fig. 16. Mode decomposition of the penny-shaped crack under mixed mode in Fig. 14. The stress intensity factor marked by superscript "a" is the solution of Fig. 15 when numerical solution is used for the auxiliary field. Those indicated by "b", "c", and "d" are the solutions when the plane strain asymptotic solutions are employed for the auxiliary field: "b": the divergence term being neglected in Eq. (25); "c": obtained by the method from Gosz et al. (1998); "d": the present method.

the finite element model with four rings is used to examine the mode decomposition employing the asymptotic auxiliary fields in a coarse mesh. Here, the three stress intensity factors K_I, K_{II}, and K_{III} are obtained from the two-state integrals with three asymptotic auxiliary fields for Mode I, Mode II, and Mode III, respectively. The solution is compared with the reference solution obtained by using the numerical auxiliary fields. The stress intensity factors calculated in the areas containing annular rings for domain integral (25) along the crack front show path independence with respect to the integration paths or rings. In Fig. 16, the average values of the stress intensity factors are plotted in terms of the angle from x axis for four solutions: the stress intensities marked by "a" is the reference solution of Fig. 15 (four rings), that is, with the numerical solution being taken for the auxiliary field; those indicated by "b", "c", and "d" are the solutions with plane strain asymptotic field being taken for the auxiliary solution. Furthermore "b" indicates the solution obtained with the divergence term being neglected, "c" those obtained by the method of Gosz et al. (1988), and "d" by the present method. In this figure, the results obtained by neglecting the divergence term in the two-state integral are a little different from the reference values. One would expect that the divergence term in the two-state integral cannot be ignored for a highly curved three-dimensional crack. Note that the present solution is almost indistinguishable from the reference solution while the solution based upon the method of Gosz et al. (1998) has some deviations in K_{III}. Considering the fact that the present method provides a more straightforward scheme for calculating the divergence term (29) in the two-state integral, it may be more attractive in view of numerical computation.

5. Concluding remarks

A method of analysis, based on the conservation laws of elasticity and the fundamental relationships in fracture mechanics, has been proposed for studying axisymmetric mixed-mode cracks and three-dimen-

sional mixed-mode cracks. The method is based on the path independence of J and two-state integral. Path independence of J and two-state integrals enables us to compute the individual stress intensity factors accurately and efficiently from the domain integral expression. The solution procedure has been established and shown to be computationally efficient and operationally simple: it involves only the choice of appropriate auxiliary solutions in the form of numerical solutions or the plane-strain asymptotic solution, and the subsequent calculation of J and two-state integrals with the aid of the domain integral expression. The asymptotic auxiliary fields for the plane-strain problems are successfully implemented to decompose three-dimensional mixed-mode crack, and a simple method is proposed to evaluate the divergence term in the two-state integral. The results for the stress intensity factors decomposed by the present method are found to be in an excellent agreement with the reference solutions obtained with the numerical auxiliary fields.

Acknowledgements

The authors gratefully acknowledge the financial support by the Korea Research Foundation (grant no. 1998-018-E00049) in the course of this study.

References

Benthem, J.P., Koiter, W.T., 1973. Asymtotic approxiations to crack problems. Method of Analysis and Solutions of Crack Problems. Noordhoff, Holland.

Budiansky, B., Rice, J.R., 1973. Conservation laws and energy release rate. ASME J. Appl. Mech. 40, 201–203.

Bui, H.D., 1983. Associated path independent J integrals for separating mixed modes. J. Mech. Phys. Solids 31, 439–448.

Chen, F.H.K., Shield, R.T., 1977. Conservation laws in elasticity of the J integral type. J. Appl. Math. Phys. (ZAMP) 28, 1–22.

Choi, N.Y., Earmme, Y.Y., 1992. Evaluation of stress intensity factors in circular arc-shaped interfacial crack using L integral. Mech. Mater. 12, 141–153.

Ernst, H.A., Rush, P.J, McCabe, D.E., 1994. Resistance curve analysis of surface cracks. Fracture Mechanics. vol. 24. ASTM STP 1207, pp. 389–409.

Eshelby, J.D., 1956. The continuum theory of lattice defects. Solid State Phys. 3, 79–144.

Gosz, M., Dolbow, J., Moran, B., 1998. Domain integral formulation for stress intensity factor computation along curved three-dimensional interface cracks. Int. J. Solids Struct. 35, 1763–1783.

Hartranft, R.J., Sih, G.C., 1973. Solving edge and surface crack problems by an alternating method. Method of Analysis and Solutions of Crack Problems. Noordhoff, Holland.

Hibbitt, H.D., Karlsson, B., Sorensen, E.P., 1997. ABAQUS user's manual. Hibbitt, Karlsson and Sorensen, Providence, RI.

Hong, C.C., Stern, M., 1978. The computation of stress intensity factors in dissimilar materials. J. Elast. 8, 21–30.

Hutchinson, J.W., 1968. Singular behavior at the end of a tensile crack in a hardening material. J. Mech. Phys. Solids 16, 13–31.

Hutchinson, J.W., Mear, M.E., Rice, J.R., 1987. Crack paralleling an interface between dissimilar materials. ASME J. Appl. Mech. 54, 828–832.

Im, S., Kim, K.S., 2000. Application of the two-state M integral for computing an intensity factor of a singular near-tip field for a generic composite wedge. J. Mech. Phys. Solids 48, 129–151.

Knowles, J.K., Sternberg, E., 1972. On a class of conservation laws in linearized and finite elastostatics. Arch. Rational Mech. Anal. 7, 55–129.

Kassir, M.K., Sih, G.C., 1974. Three-dimensional crack problems. Mechanics of Fracture, vol. 2. Noordhoff, Holland.

Kuo, A., 1987. On the use of a path-independent line integral for axisymmetric cracks with nonaxisymmetric loading. ASME J. Appl. Mech. 54, 833–837.

Li, F.Z., Shih, C.F., Needleman, A., 1985. A comparison of methods for calculating energy release rates. Engng. Fract. Mech. 21, 405–421.

Moran, B., Shih, C.F., 1987. Crack tip and associated domain integrals from momentum and energy balance. Engng. Fract. Mech. 27, 615–642.

Nahta, R., Moran, B., 1993. Domain integrals for axisymmetric interface crack problems. Int. J. Solids Struct. 30, 2027–2040.

Nakamura, T., Parks, D.M., 1989. Antisymmetrical 3-d stress field near the crack front of a thin elastic plate. Int. J. Solids Struct. 25, 1411–1426.

Nakamura, T., 1991. Three-dimensional stress fields of elastic interface cracks. ASME J. Appl. Mech. 58, 939–946.
Nikishkov, G.P., Atluri, S.N., 1987a. Calculation of fracture mechanics parameters for an arbitrary three-dimensional crack by the equivalent domain integral method. Int. J. Numer. Methods Engng. 24, 1801–1821.
Nikishkov, G.P., Atluri, S.N., 1987b. An equivalent domain integral method for computing crack tip integral parameters in nonelastic, thermo-mechanical fracture. Engng. Fract. Mech. 26, 851–867.
Rice, J.R., 1968. A path-independent integral and approximate analysis of strain concentrations by notches and cracks. ASME J. Appl. Mech. 35, 379–386.
Sharobeam, M.H., Landes, J.D., 1995. A single specimen approach for *J*-integral evaluation for semi-elliptical surface cracks. Fracture Mechanics. vol. 25. ASTM STP 1220, pp. 397–414.
Shih, C.F., Asaro, R.J., 1988. Elastic–plastic analysis of cracks on bimaterial interfaces: part II-structure of small-scale yielding fields. ASME J. Appl. Mech. 55, 299–316.
Stern, M., Becker, E.B., Dunham, R.S., 1976. A contour integral computation of mixed mode stress intensity factors. Int. J. Fracture 12, 359–368.
Wang, S.S., Yau, J.F., 1981. Interfacial cracks in adhesively bonded scarf joints. AIAA 19, 1350–1356.
Yang, M., Kim, K., 1993. The behavior of sub-interface cracks with crack-face contact. Engng. Fract. Mech. 44, 155–165.
Yau, J.F., Wang, S.S., Corten, H.T., 1980. A mixed mode crack analysis of isotropic solids using conservation laws of elasticity. ASME J. Appl. Mech. 47, 335–341.